Journal of Power Sources 426 (2019) 162–168

Contents lists available at ScienceDirect

Journal of Power Sources

journal homepage: www.elsevier.com/locate/jpowsour

In situ electrochemical surface modification for high-voltage $LiCoO_2$ in lithium ion batteries

Jungwoo Lim, Aram Choi, Hanseul Kim, Sung Wook Doo, Yuwon Park, Kyu Tae Lee*

School of Chemical and Biological Engineering, Institute of Chemical Processes, Seoul National University, Gwanak-gu, Seoul, 08826, South Korea

HIGHLIGHTS

- Introducing a simple *in situ* electrochemical surface modification method.
- Electrochemical formation of MgF_2 coating layers on a $LiCoO_2$ surface.
- Clarifying the formation mechanism of MgF_2 coating layers from $Mg(ClO_4)_2$.
- Role of $LiPF_6$ salt and polyvinylidene fluoride binder in the formation of MgF_2.
- Suppressing Co dissolution, leading to the improved electrochemical performance.

ARTICLE INFO

Keywords:
Cathode electrolyte interphase
Lithium cobalt oxide
Cathode
Surface modification
Lithium ion batteries

ABSTRACT

High-voltage $LiCoO_2$ has been revisited to improve the energy density of lithium ion batteries. $LiCoO_2$ can deliver the reversible capacity of about 200 mA h g^{-1} when the upper cut-off voltage increases to 4.55 V (vs. Li/Li^+). However, the high upper cut-off voltage causes the severe failures of $LiCoO_2$ such as structural degradation, electrolyte decomposition, and Co dissolution. Various surface-modified $LiCoO_2$ materials have been introduced to suppress electrolyte decomposition and Co dissolution, thereby leading to the improved electrochemical performance. Most of the coated $LiCoO_2$ materials are obtained through a conventional coating process such as sol-gel synthesis, which is complex and high-cost. In this paper, the *in situ* electrochemical coating method is introduced as a simple and low-cost coating process, where the electrolyte additive of Mg salts is electrochemically decomposed to form a MgF_2-based coating layer on the $LiCoO_2$ surface. $LiCoO_2$ electrochemically coated with MgF_2 suppresses Co dissolution in electrolytes, resulting in excellent electrochemical performance such as high reversible capacity of 198 mA h g^{-1} and stable cycle performance over 100 cycles in the voltage range between 3 and 4.55 V (vs. Li/Li^+) at 45 °C. The formation mechanism of MgF_2 is also demonstrated through *ex situ* XPS and XANES analyses.

1. Introduction

Lithium ion batteries are the most widely used energy storage devices for portable electronics such as laptops and mobile phones. However, emerging electronics consume more energy, and consequently require the higher energy density of lithium ion batteries. In this connection, there has been much effort to improve the energy density of cathode materials for lithium ion batteries [1,2]. For example, Ni-rich [3–6] and Li, Mn-rich layered oxide materials [7–11] have been investigated because of their high reversible capacities. $LiCoO_2$ has also been revisited to deliver the reversible capacity of about 200 mA h g^{-1} that is enabled by increasing upper cut-off voltage to 4.55 V (vs. Li/Li^+) [12,13]. A change in the upper cut-off voltage, however, causes the severe degradation of $LiCoO_2$, resulting in poor electrochemical performance except for the high reversible capacity. For example, the irreversible phase transition is known to occur from O3 to O1 through H1-3 above 4.5 V vs. Li/Li^+ [14,15]. The surface of $LiCoO_2$ is transformed into Li-deficient spinel-like phases such as Co_3O_4 [16,17] and $Li_xCo_2O_4$ [18] during cycling, leading to increase in a charge transfer resistance. In addition, severe anodic electrolyte decomposition occurs above 4.5 V vs. Li/Li^+, resulting in the formation of thick passivation layer on the cathode surface [19]. This layer is called cathode electrolyte interphase (CEI). Finally, Co dissolution in electrolytes is accelerated at high voltages [20].

The structural degradation of $LiCoO_2$ at high voltages is known to be mitigated by the addition of various dopants such as Mg^{2+} [21,22],

* Corresponding author.
E-mail address: ktlee@snu.ac.kr (K.T. Lee).

https://doi.org/10.1016/j.jpowsour.2019.04.011
Received 30 May 2018; Received in revised form 2 March 2019; Accepted 3 April 2019
Available online 15 April 2019
0378-7753/

Al^{3+} [23,24], and Ti^{4+} [25], leading to improved cycle performance. Surface modification of $LiCoO_2$ is also efficient to suppress electrolyte decomposition [26] and Co dissolution [27]. In particular, the surface-modified $LiCoO_2$ with metal fluorides such as AlF_3 [28] and MgF_2 [29] showed promising electrochemical performance. Most of the metal fluoride-coated cathode materials are obtained through conventional wet coating processes including sol-gel synthesis, which require the additional coating steps after the solid state synthesis of $LiCoO_2$ [30–32]. This conventional coating method is relatively complex and high-cost. In this report, we introduce the *in situ* electrochemical coating method that the electrolyte additive of Mg salts is electrochemically decomposed to form the MgF_2-based CEI layer on the $LiCoO_2$ surface. This *in situ* electrochemical coating method is simple and low-cost. $LiCoO_2$ electrochemically coated with MgF_2 suppresses Co dissolution in electrolytes, resulting in excellent electrochemical performance such as high reversible capacity of 198 mA h g^{-1} and stable cycle performance over 100 cycles in the voltage range between 3 and 4.55 V vs. Li/Li^+ at 45 °C. We also clarified the formation mechanism of MgF_2 coating layers, where both $LiPF_6$ salt and polyvinylidene fluoride (PVDF) binder are provided as a source of fluorine in MgF_2.

2. Experimental section

2.1. Synthesis and material characterization

Li_2CO_3 and $CoCO_3$ (0.515 : 1 as a molar ratio) were mixed by wet-milling with ethanol at 300 rpm for 1 h. The mixed precursors were heated at 900 °C for 10 h. X-ray diffraction (XRD) patterns of $LiCoO_2$ were collected using a D2 phaser (bruker) with Cu-Kα radiation (λ = 1.5418 Å). Field emission scanning electron microscopy (FE-SEM) and high-resolution transmission electron microscopy (HR-TEM) with energy dispersive spectroscopy (EDS) were carried out using a JSM-6700F (JEOL) and JEM-2100F (JEOL), respectively. The cross sectional TEM images were obtained using an ion slicer (EM-09100 IS, JEOL). X-ray Absorption Near-Edge Structure (XANES) spectra were obtained on the PLS-II 6D beamline at the Pohang Accelerator Laboratory (PAL). X-ray Photoelectron Spectroscopy (XPS, K-alpha, Thermo scientific) analyses were performed after etching for 50 s to remove surface contaminations. The amount of Co dissolution in electrolytes was measured using inductively coupled plasma – mass spectroscopy (ICP–MS, Agilent 7900). After charging $LiCoO_2$ to 4.55 V (vs. Li/Li^+), cells were disassembled and $LiCoO_2$ electrodes were recovered. Then, charged electrodes were stored in 5 ml of 1.3 M $LiPF_6$ dissolved in ethylene carbonate (EC)/ethyl-methyl carbonate (EMC)/dimethyl carbonate (DMC) solution (3/4/3, v/v/v) at 85 °C for 15 days. Time of flight secondary ion mass spectroscopy (TOF-SIMS, Ion-TOF) was carried out using the $LiCoO_2$ electrode cycled with 1.3 M $LiPF_6$ in EC/EMC/DMC containing $LiClO_4$ and $Mg(ClO_4)_2$.

2.2. Electrochemical characterization

Electrodes were prepared by mixing active materials ($LiCoO_2$), carbon black (Super P), and PVDF binder in a weight ratio of 8:1:1. The slurries were casted on aluminum current collectors. Activated carbon (AC) electrodes were prepared in a form of free-standing films composed of AC, carbon Super P, polytetrafluoroethylene (PTFE) binder in a weight ratio of 8:1:1.

Electrochemical performance of $LiCoO_2$ was evaluated using half cells (2032-type coin cells) comprising $LiCoO_2$, Li metal, 1.3 M of $LiPF_6$ dissolved in EC/EMC/DMC solution (3/4/3, v/v/v) containing various amounts of $Mg(ClO_4)_2$. Pre-cycling was conducted in the voltage range of 3–4.4 V (vs. Li/Li^+) at 15 mA g^{-1} (0.1C) and 30 °C for 5 cycles. After pre-cycling, galvanostatic cycling was performed in the voltage ranges of 3–4.4 and 3–4.55 V (vs. Li/Li^+) at 45 and 60 °C. The current density was 150 mA g^{-1} (1C). In addition, the electrochemical performance of full cells comprising $LiCoO_2$ cathode and graphite anode was examined to investigate the Mg deposition on the graphite surface. The N/P ratio of full cells was 1.15. Full cells were cycled in the voltage range of 2.9–4.3 V.

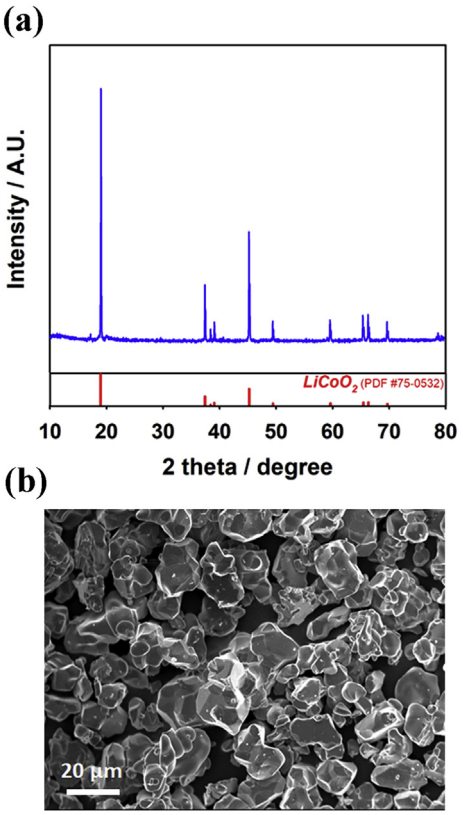

Fig. 1. (a) XRD pattern and (b) FE-SEM image of $LiCoO_2$.

3. Results and discussion

3.1. In situ surface modification of $LiCoO_2$

$LiCoO_2$ powders were synthesized through a conventional solid state method. Negligible impurities were observed in the XRD pattern of $LiCoO_2$ powders (Fig. 1a). $LiCoO_2$ powders are a few tens of micrometers in size, as shown in the SEM image of $LiCoO_2$ powders (Fig. 1b). After assembling a half cell comprising $LiCoO_2$, Li metal, and 1.3 M $LiPF_6$ dissolved in EC/EMC/DMC solution (3/4/3, v/v/v) with and without 0.03 M $Mg(ClO_4)_2$, we performed a galvanostatic cycling in the voltage range of 3–4.4 V (vs. Li/Li^+) at 15 mA g^{-1} (0.1C) and 30 °C for 5 cycles. The cells were disassembled after cycling, and then we carried out *ex situ* TEM and XPS analyses for cycled $LiCoO_2$ electrodes to observe changes in the $LiCoO_2$ surface after cycling. Fig. 2a and b shows the cross sectional TEM image and corresponding EDS mapping image of $LiCoO_2$ after 5 cycles. Mg was uniformly concentrated on the $LiCoO_2$ surface, and the thickness of Mg-containing layer was a few tens of nanometers. Fig. 2c–f shows the XPS spectra of Mg 1s and F 1s for the $LiCoO_2$ cycled with bare and $Mg(ClO_4)_2$-containing electrolytes. When 0.03 M $Mg(ClO_4)_2$ was added in the electrolyte, a peak appeared at 1305.8 eV in the XPS spectrum of Mg 1s (Fig. 2c). This peak corresponds to MgF_2 [33], which indicates that $Mg(ClO_4)_2$ was decomposed to form MgF_2 on the $LiCoO_2$ surface. Regardless of the addition of Mg $(ClO_4)_2$, we also observed three peaks at 685.5 eV, 686.6 eV, and 688.0 eV in the XPS spectra of F 1s, corresponding to metal fluorides, $Li_xPF_yO_z$ and PVDF binder, respectively (Fig. 2d, f) [10,34,35]. PF_6^- is known to be decomposed into F^- and PF_5 at high voltages, which is followed by the reaction between Li^+ and F^- to form LiF [36]. This

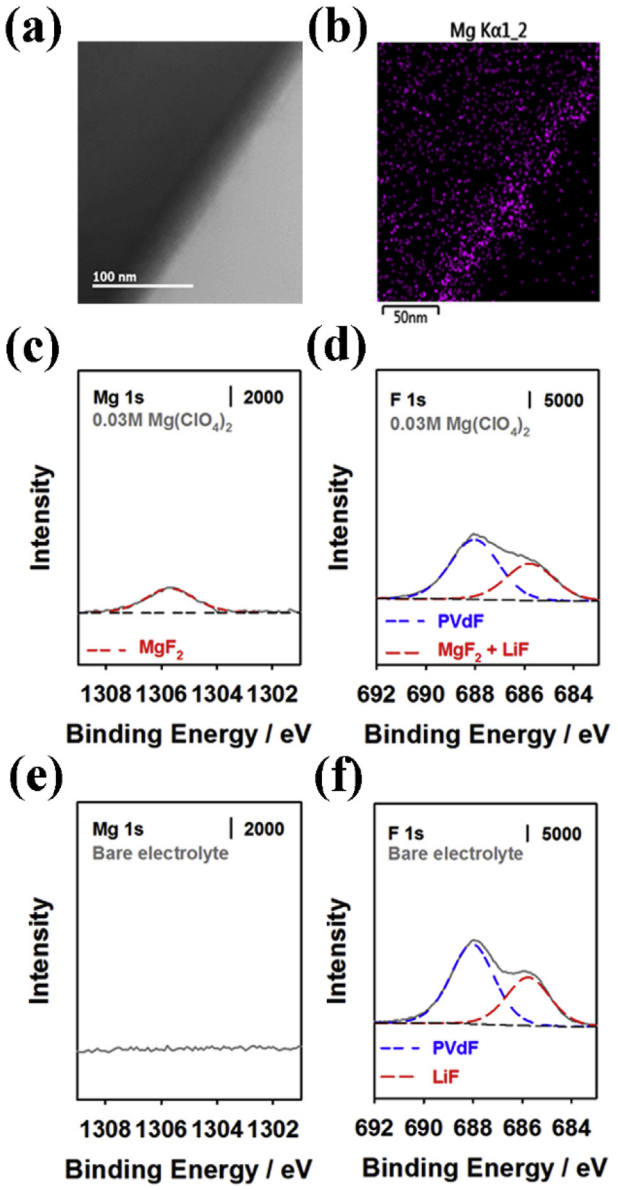

Fig. 2. (a) Cross-sectional TEM image and (b) corresponding EDS mapping image of the $LiCoO_2$ cycled with $Mg(ClO_4)_2$ for 5 cycles. XPS spectra of (c) Mg 1s and (d) F 1s for the $LiCoO_2$ cycled with $Mg(ClO_4)_2$-containing electrolytes. XPS spectra of (e) Mg 1s and (f) F 1s for the $LiCoO_2$ cycled with bare electrolytes.

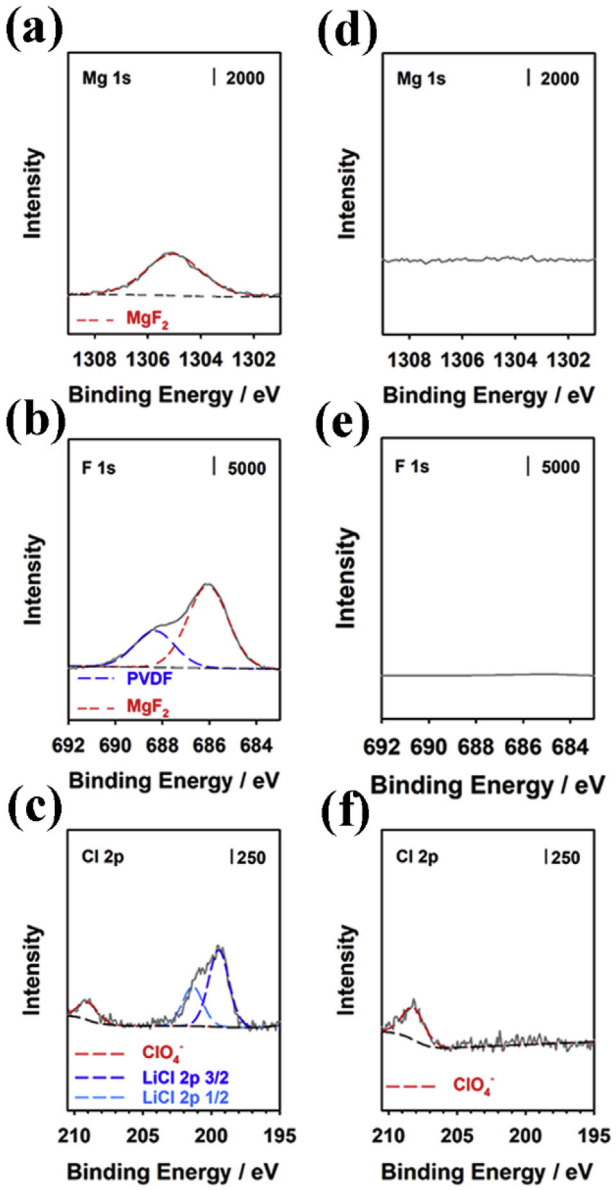

Fig. 3. XPS spectra of (a) Mg 1s, (b) F 1s, and (c) Cl 2p for the $LiCoO_2$ electrodes prepared with a PVDF binder after 5 cycles. XPS spectra of (d) Mg 1s, (e) F 1s, and (f) Cl 2p for the $LiCoO_2$ electrodes prepared with a PAA binder after 5 cycles. The electrolyte was 1.0 M $LiClO_4$ and 0.03 M $Mg(ClO_4)_2$ dissolved in EC/EMC/DMC solution.

suggests that the peak at 685.7 eV for the bare electrolyte is due to the formation of LiF from $LiPF_6$. The binding energies of F 1s in LiF and MgF_2 are very close, such as 685.5 eV for LiF [37] and 685.52 eV for MgF_2 [38]. Therefore, the peak at 685.7 eV for the $Mg(ClO_4)_2$-containing electrolyte should be considered to be attributed to both LiF and MgF_2 derived from $LiPF_6$ and $Mg(ClO_4)_2$ [36–39]. Wagner et al. reported that the formation of MgF_2 is thermodynamically more favorable than that of LiF when PF_6^- is decomposed in the electrolyte containing both Mg^{2+} and Li^+ ions [39]. This supports that the CEI layer of $LiCoO_2$ contains both LiF and MgF_2 when $LiPF_6$ and $Mg(ClO_4)_2$ are dissolved in the electrolyte.

We performed additional *ex situ* XPS analysis to demonstrate the formation mechanism of MgF_2 on the $LiCoO_2$ surface. Fig. 3 compares the XPS spectra of Mg 1s, F 1s, and Cl 2p for the $LiCoO_2$ electrodes prepared with PVDF and polyacrylic acid (PAA) binders after 5 cycles, where the electrolyte was 1.0 M $LiClO_4$ and 0.03 M $Mg(ClO_4)_2$ dissolved in EC/EMC/DMC solution. Note that there was no fluorine source in the electrolyte for this case because $LiClO_4$ was used instead of $LiPF_6$ as a Li salt. As expected, no MgF_2 was formed on the $LiCoO_2$ surface, when PAA was used as a binder. However, interestingly, MgF_2 was formed on the $LiCoO_2$ surface when PVDF was used as a binder, despite the fact that there was no fluorine source in the electrolyte. This indicates that PVDF was decomposed and reacted with Mg^{2+} in the electrolyte, leading to the formation of MgF_2, although PVDF are chemically very stable. Moreover, we performed *ex situ* TOF-SIMS analysis to support the formation of MgF_2 on the $LiCoO_2$ surface (Supplementary Information, Fig. S1). Fig. S1 shows the TOF-SIMS spectrum of the $LiCoO_2$ electrode cycled with 1.0 M $LiClO_4$ in EC/EMC/DMC (3/4/3) containing 0.03 M $Mg(ClO_4)_2$ and PVDF binder. We observed the peak of MgF^- at *m/z* 43 in the TOF-SIMS spectrum in the negative ion mode. The fragment of MgF^- was obtained from MgF_2, revealing that MgF_2 was formed on the on the $LiCoO_2$ surface. This is consistent with the *ex situ* XPS analysis (Fig. 3).

PVDF is known to react with strong bases such as organic bases,

LiOH, and LiO_2 through chemical dehydrofluorination [40,41], resulting in the release of F^- In this connection, we propose the formation mechanism of MgF_2 derived from PVDF as follows. H_2O reacts with Li^+ and e^- in the electrolyte, leading to the formation of LiOH and H_2 [42]. Then, OH^- abstracts the proton from the PVDF, followed by release of F^- to form a conjugated double bond [41]. Finally, F^- reacts with Mg^{2+} to form MgF_2. Therefore, we suggest two possible ways of forming MgF_2 on the $LiCoO_2$ surface when $LiPF_6$ and PVDF are used as Li salt and binder, respectively. One is due to the decomposition of $LiPF_6$ [43]. The other is attributed to the decomposition of PVDF through dehydrofluorination [44–46]. These decompositions release F^-, followed by the reaction with Mg^{2+} to form MgF_2.

(i) When $LiPF_6$ was used as a Li salt in the electrolyte,

$$2PF_6^- \rightarrow 2F^- + 2PF_5 \quad (1)$$

$$Mg^{2+} + 2F^- \rightarrow MgF_2 \quad (2)$$

(ii) When PVDF was used as a binder,

$$Li^+ + e^- + H_2O \rightarrow LiOH + 1/2H_2 \quad (3)$$

$$(–CH_2–CF_2–)_n\ (PVDF) + OH^- \rightarrow (–CH=CF-)_n + H_2O + F^- \quad (4)$$

$$Mg^{2+} + F^-\ from\ PVDF \rightarrow MgF_2 \quad (5)$$

Moreover, we performed *ex situ* XANES analysis to clarify the possibility of Mg doping into $LiCoO_2$. $LiCoO_2$ was charged to 4.4 V (vs. Li/Li^+) using a Li half-cell comprising $LiCoO_2$ working electrode, Li metal counter electrode, and $LiPF_6$ dissolved in EC/EMC/DMC (3/4/3, v/v/v), resulting in the formation of Li-deficient $Li_{1-x}CoO_2$. The charging profile is presented in Fig. 4a. After charging, the cell was disassembled and the Li-deficient $Li_{1-x}CoO_2$ electrode was recovered. Then, we reassembled a Mg half-cell comprising $Li_{1-x}CoO_2$ working electrode, activated carbon (AC) counter electrode, and 0.3 M $Mg(ClO_4)_2$ dissolved in EC/EMC/DMC (3/4/3, v/v/v). The Mg half-cell of $Li_{1-x}CoO_2$ was discharged to −1.3 V (vs. AC). The potential of the AC electrode in the Mg half-cell was calibrated using the ferrocene/ferrocenium (Fc/Fc^+) redox couple [47]. The potential of −1.3 V (vs. AC) in a Mg half-cell corresponds to approximately 2 V (vs. Li/Li^+) in a Li half-cell. Considering the sluggish kinetics of Mg^{2+} intercalation, a very small current density of 1.5 mA g^{-1} (0.01C) was applied during discharge. Fig. 4b shows the discharge profile of $Li_{1-x}CoO_2$ using the Mg half-cell. $Li_{1-x}CoO_2$ delivered negligible discharge capacity as much as approximately 6 mA h g^{-1}. This indicates that a negligible amount of Mg^{2+} was intercalated into $Li_{1-x}CoO_2$. This is supported by *ex situ* XANES analysis. Fig. 4c shows the normalized Co K-edge XANES spectra of pristine $LiCoO_2$ (black line), $Li_{1-x}CoO_2$ that is charged to 4.4 V (vs. Li/Li^+) using a Li half-cell (red line), and $[Li_{1-x}Mg_y]CoO_2$ that is discharged to −1.3 V (vs. AC) using a Mg half-cell (blue line). After charging, the main edge shifted to higher energy, indicating that the oxidation state of Co increased during charge. However, no shift was observed in the main edge after discharge, implying that there was no change in the oxidation state of Co during discharge. This supports that Mg^{2+} was not intercalated into $Li_{1-x}CoO_2$. Therefore, the additive of Mg $(ClO_4)_2$ does not contribute to the structural modification of $LiCoO_2$ through the electrochemical intercalation of Mg^{2+} but plays a role in the surface medication of $LiCoO_2$ by the formation of MgF_2-based CEI layer.

3.2. Role of $Mg(ClO_4)_2$ in electrochemical performance

Fig. 5 shows the cycle performance of $LiCoO_2$ with various amounts of $Mg(ClO_4)_2$ in the voltage ranges of 3–4.4 V and 3–4.55 V (vs. Li/Li^+) at 150 mA g^{-1} (1C) and 45 °C. The corresponding voltage profiles were

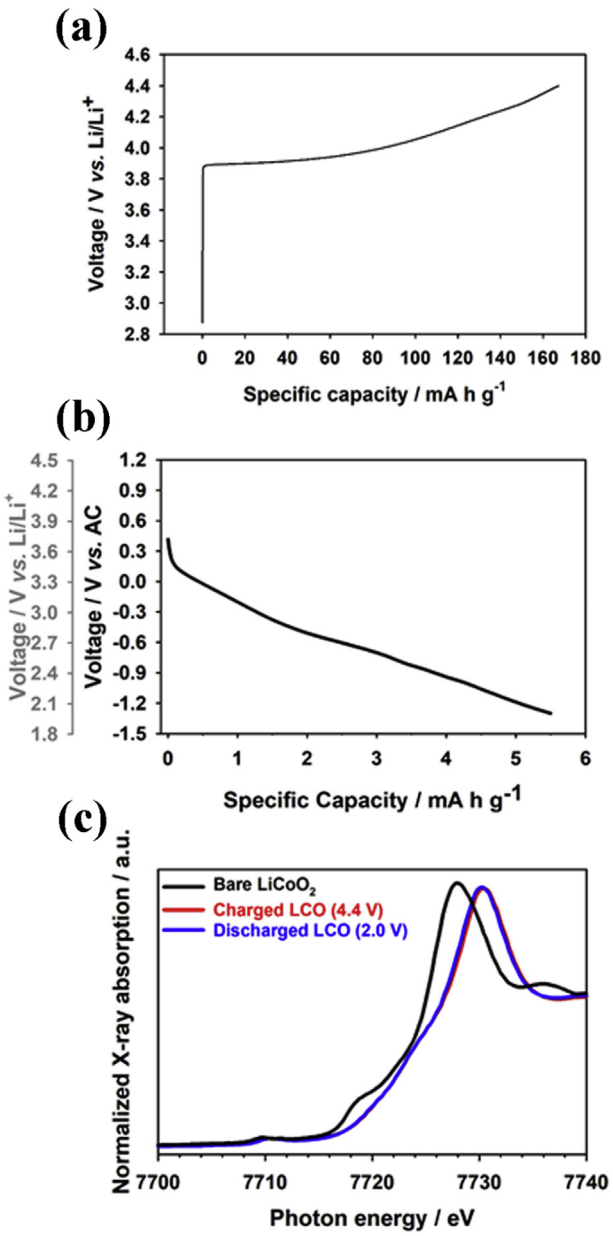

Fig. 4. (a) Charge profile of $LiCoO_2$ using a Li half-cell. (b) Discharge profile of delithiated $Li_{1-x}CoO_2$ using an Mg half-cell. (c) Normalized Co K-edge XANES spectra of $LiCoO_2$.

displayed in Fig. 6. As the amount of $Mg(ClO_4)_2$ increased from 0 to 0.03 M, $LiCoO_2$ exhibited less increase in charge and discharge polarization with increasing cycle number, resulting in more stable cycle performance. When $Mg(ClO_4)_2$ was not added in the electrolyte, bare $LiCoO_2$ showed the poor capacity retentions of *ca.* 72.4 and 59.6% in the voltage ranges of 3–4.4 V and 3–4.55 V (vs. Li/Li^+) after 100 cycles, respectively. However, 0.03 M $Mg(ClO_4)_2$ remarkably improved the cycle performance of $LiCoO_2$ such as the capacity retentions of *ca.* 86.7 and 73% in the voltage ranges of 3–4.4 V and 3–4.55 V (vs. Li/Li^+) after 100 cycles, respectively. Moreover, $Mg(ClO_4)_2$ improved the cycle performance of $LiCoO_2$ even at 60 °C, as shown in Fig. 7.

In order to elucidate the role of $Mg(ClO_4)_2$ in the improved cycle performance of $LiCoO_2$, we measured the amounts of Co dissolution after storing charged $LiCoO_2$ in the electrolyte at 85 °C for 15 days. One of the failure mechanisms of $LiCoO_2$ at high voltages is known to be Co dissolution in electrolytes during cycling. $LiPF_6$ reacts with H_2O, leading to the formation of highly corrosive HF [43,48]. Then, HF

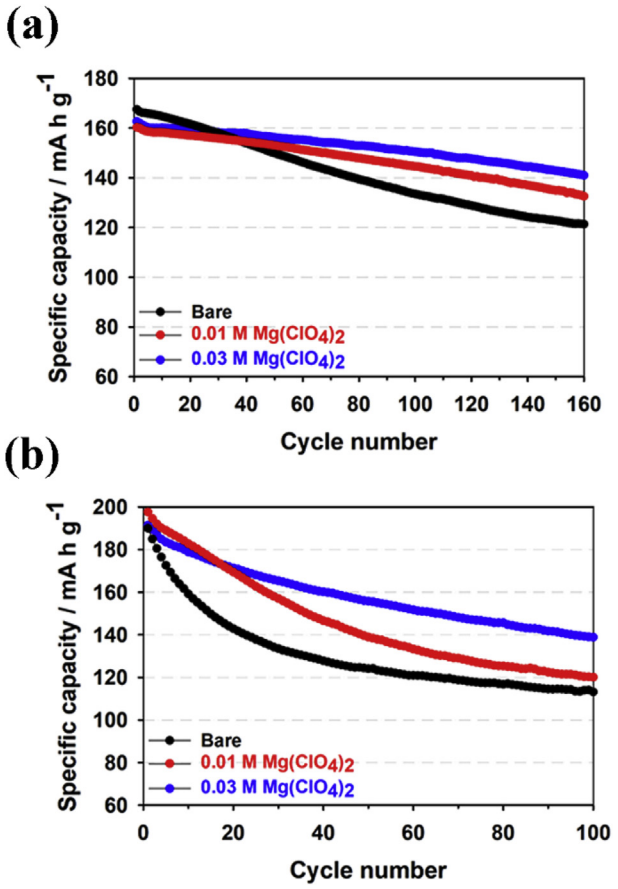

Fig. 5. Cycle performance of $LiCoO_2$ cycled with bare, 0.01 M $Mg(ClO_4)_2$-containing, and 0.03 $Mg(ClO_4)_2$-containing electrolytes in the voltage ranges of (a) 3–4.4 and (b) 3–4.55 V (vs. Li/Li^+) at 150 mA g^{-1} (1C) and 45 °C.

dissolves Co from $LiCoO_2$. As shown in Fig. 8, $Mg(ClO_4)_2$ substantially suppressed Co dissolution of $LiCoO_2$ in electrolytes. This is attributed to that MgF_2-based CEI layer derived from $Mg(ClO_4)_2$ protects $LiCoO_2$ surface from HF attacks. As a result, $Mg(ClO_4)_2$ improved the cycle performance of $LiCoO_2$.

Moreover, we have examined the full cell comprising $LiCoO_2$ cathode and graphite anode to investigate Mg deposition on the graphite surface during cycling. The N/P ratio of full cells was 1.15. The electrochemical performance of full cells was examined with two kinds of electrolytes, such as 1.3 M $LiPF_6$ in EC/EMC/DMC containing 0.03 M $Mg(ClO_4)_2$ (denoted as baseline) and 1.3 M $LiPF_6$ in EC/EMC/DMC containing 0.03 M $Mg(ClO_4)_2$ and 2 wt% vinylene carbonate (VC) (denoted as baseline + VC). After 5 cycles, full cells were disassembled and electrodes were washed with DMC solvent. The surfaces of $LiCoO_2$ cathode and graphite anode were then analyzed using SEM with EDS. As shown in the EDS spectra of the full cell with the baseline electrolyte (Supplementary Information, Figs. S2 and S3), a very small peak of Mg was observed on the graphite surface. However, the Mg peak of the $LiCoO_2$ surface was much more intense than that of the graphite surface. This implies that $MgClO_4$ was decomposed mostly on the $LiCoO_2$ surface, forming MgF_2-based CEI layer, whereas a small amount of Mg was deposited on the graphite surface. In addition, a negligible amount of Mg was observed on the graphite surface when VC additive was added in the electrolyte (Supplementary Information, Figs. S4 and S5). This indicates that the VC additive formed a stable SEI layer on the graphite anode surface and the SEI layer suppressed the deposition of Mg in the full cell during cycling. As a result, the full cell with VC showed better cycle performance than the full cell without VC (Supplementary Information, Fig. S6).

4. Conclusion

We introduced the *in situ* electrochemical coating method that the electrolyte additive of Mg salts is electrochemically decomposed to form a MgF_2-based coating layer on the $LiCoO_2$ surface. We clarified the formation mechanism of MgF_2 through *ex situ* XPS and XANES analyses. When $Mg(ClO_4)_2$ was added in the electrolyte containing $LiPF_6$. PF_6^-

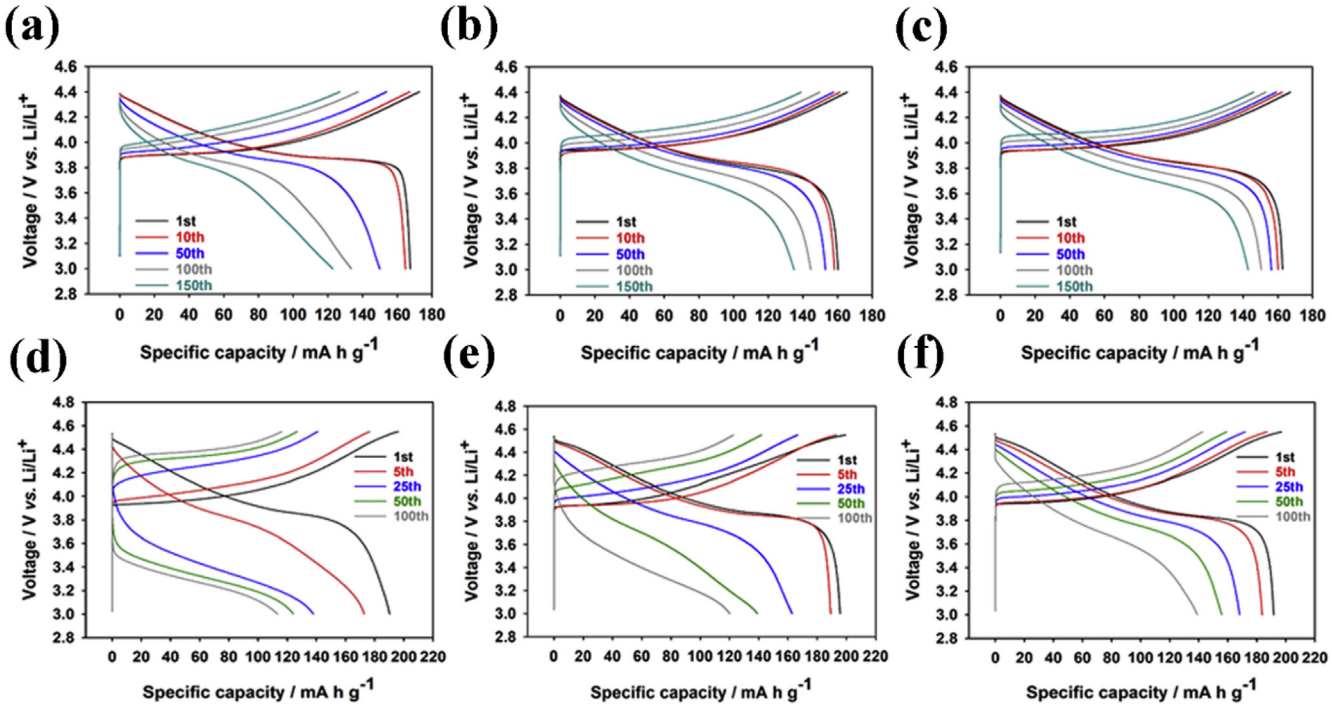

Fig. 6. Voltage profiles in the voltage range of 3–4.4 V (vs. Li/Li^+) at 45 °C: (a) bare, (b) 0.01 M $Mg(ClO_4)_2$, and (c) 0.03 M $Mg(ClO_4)_2$. Voltage profiles in the voltage range of 3–4.55 V (vs. Li/Li^+) at 45 °C: (d) bare, (e) 0.01 M $Mg(ClO_4)_2$, and (f) 0.03 M $Mg(ClO_4)_2$.

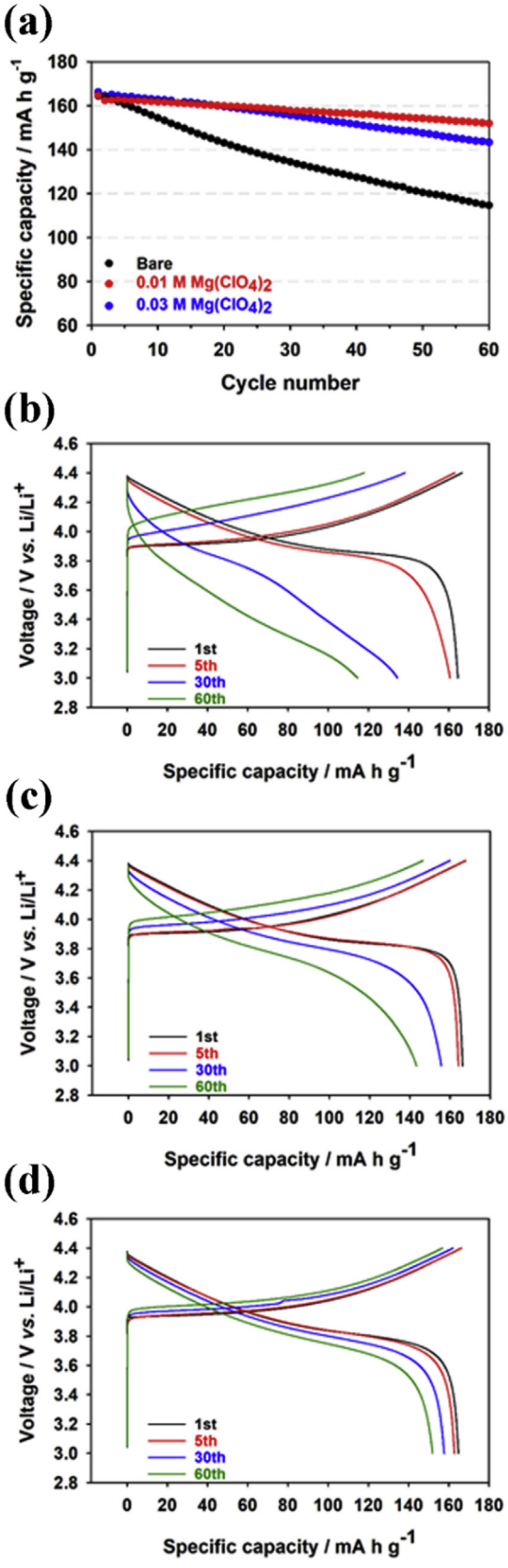

Fig. 7. (a) Cycle performance of $LiCoO_2$ cycled with bare, 0.01 M $Mg(ClO_4)_2$-containing, and 0.03 $Mg(ClO_4)_2$-containing electrolytes in the voltage range of 3–4.4 V (vs. Li/Li^+) at 60 °C. Corresponding voltage profiles: (b) bare, (c) 0.01 M $Mg(ClO_4)_2$, and (d) 0.03 M $Mg(ClO_4)_2$.

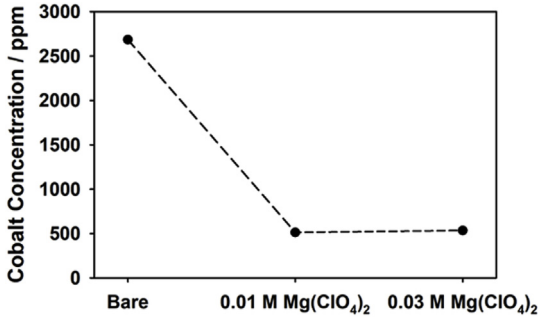

Fig. 8. The amounts of Co dissolution after storing charged $LiCoO_2$ electrodes in various electrolytes at 85 °C for 15 days. The electrodes were charged to 4.55 V (vs. Li/Li^+).

was decomposed into F^- and PF_5 at high voltages, which is followed by the reaction between Mg^{2+} and F^- to form MgF_2 on the $LiCoO_2$ surface. Moreover, PVDF binder was decomposed through chemical dehydrofluorination. The released F^- reacted with Mg^{2+} to form MgF_2 on the $LiCoO_2$ surface. The thickness of MgF_2-based coating layer was a few tens of nanometers.

$LiCoO_2$ electrochemically coated with MgF_2 suppressed Co dissolution in electrolytes. As a result, MgF_2-coated $LiCoO_2$ showed excellent electrochemical performance including the high reversible capacity of 198 mA h g^{-1} and stable cycle performance over 100 cycles in the voltage range of 3–4.55 V (vs. Li/Li^+) at 45 °C. We believe that this simple electrochemical coating method can be extended to various metal fluorides-coated cathode materials.

Acknowledgements

This work was supported in part by the National Research Foundation of Korea (NRF) grant funded by the Korea government (MSIT) (NRF-2016R1A2B3015956 and NRF-2018R1A5A1024127), and by Technology Development Program to Solve Climate Changes (NRF-2018M1A2A2063345) through NRF funded by Ministry of Science and ICT

Appendix A. Supplementary data

Supplementary data related to this article can be found at https://doi.org/10.1016/j.jpowsour.2019.04.011.

References

[1] Aijun Zhou, Qin Liu, Yi Wang, Weihang Wang, Xu Yao, Wentao Hu, Long Zhang, Xiqian Yu, Jingze Li, Li Hong, J. Mater. Chem. 5 (2017) 24361–24370.
[2] Limin Zhou, Kai Zhang, Zhe Hu, Zhanliang Tao, Liqiang Mai, Yong-Mook Kang, Shu-Lei Chou, Jun Chen, Adv. Energy Mater. 8 (2018) 1701415.
[3] Florian Schipper, Evan M. Erickson, Christoph Erk, Ji-Yong Shin, Frederick Francois Chesneau, Doron Aurbach, J. Electrochem. Soc. 164 (2017) A6220–A6228.
[4] Yang Shi, Minghao Zhang, Danna Qian, Ying Shirley Meng, Electrochim. Acta 203 (2016) 154–161.
[5] Wontae Lee, Shoaib Muhammad, Taewhan Kim, Hyunchul Kim, Eunkang Lee, Mihee Jeong, Suhan Son, Jae-Hyun Ryou, Won-Sub Yoon, Adv. Energy Mater. 8 (2018) 1701788.
[6] Hanseul Kim, Aram Choi, Sung Wook Doo, Jungwoo Lim, YoungJin Kim, Kyu Tae Lee, J. Electrochem. Soc. 165 (2018) A201–A205.
[7] A. Robert Armstrong, Michael Holzapfel, Petr Novák, Christopher S. Johnson, Sun-Ho Kang, Michael M. Thackeray, Peter G. Bruce, J. Am. Chem. Soc. 128 (2006) 8694–8698.
[8] Jung-Gu Han, Sung Jun Lee, Jaegi Lee, Jeom-Soo Kim, Kyu Tae Lee, Nam-Soon Choi, ACS Appl. Mater. Interfaces 7 (2015) 8319–8329.
[9] Sangryun Kim, Woosuk Cho, Xiaobin Zhang, Yoshifumi Oshima, Jang Wook Choi, Nat. Commun. 7 (2016) 13598.
[10] Karalee Jarvis, Chih-Chieh Wang, Maria Varela, Raymond R. Unocic, Arumugam Manthiram, Paulo J. Ferreira, Chem. Mater. 29 (2017) 7668–7674.
[11] Ji-Lei Shi, Jie-Nan Zhang, Min He, Xu-Dong Zhang, Ya-Xia Yin, Hong Li, Yu-Guo Guo, Lin Gu, Li-Jun Wan, ACS Appl. Mater. Interfaces 8 (2016) 20138–20146.
[12] Aaron Liu, Li Jing, Shunmugasundaram Ramesh, J.R. Dahn, J. Electrochem. Soc. 164 (2017) A1655–A1664.

[13] Xinyi Dai, Aijun Zhou, Jin Xu, Yanting Lu, Liping Wang, Cong Fan, Jingze Li, J. Phys. Chem. C 120 (2016) 422–430.
[14] Zhaohui Chen, J.R. Dahn, Electrochim. Acta 49 (2004) 1079–1090.
[15] A. Van der Ven, M.K. Aydinol, G. Ceder, G. Kresse, J. Hafner, Phys. Rev. B 58 (1998) 2975–2987.
[16] Akira Yano, Masahiro Shikano, Atsushi Ueda, Hikari Sakaebe, Zempachi Ogumi, J. Electrochem. Soc. 164 (2017) A6116–A6122.
[17] Doron Aurbach, Boris Markovsky, Gregory Salitra, Elena Markevich, Yossi Talyossef, Maxim Koltypin, Linda Nazar, Brian Ellis, Daniella Kovacheva, J. Power Sources 165 (2007) 491–499.
[18] R.J. Gummow, D.C. Liles, M.M. Thackeray, W.I.F. David, Mater. Res. Bull. 28 (1993) 1177–1184.
[19] Jie-Nan Zhang, Qinghao Li, Yi Wang, Jieyun Zheng, Xiqian Yu, Li Hong, Energy Storage Mater. 14 (2018) 1–7.
[20] G.G. Amatucci, J.M. Tarascon, L.C. Klein, Solid State Ionics 83 (1996) 167–173.
[21] S. Levasseur, M. Ménétrier, C. Delmas, Chem. Mater. 14 (2002) 3584–3590.
[22] Aram Choi, Jungwoo Lim, Hyung-Jin Kim, Sung Chul Jung, Hyung-Woo Lim, Hanseul Lim, Mi-Sook Kwon, Young Kyu Han, Seung M. Oh, Kyu Tae Lee, Adv. Energy Mater. 8 (2018) 1702514.
[23] Seung-Taek Myung, Naoaki Kumagai, Shinichi Komaba, Hoon-Taek Chung, Solid State Ionics 139 (2001) 47–56.
[24] Kisuk Kang, Gerbrand Ceder, Phys. Rev. B 74 (2006) 094105.
[25] S. Gopukumar, Yonghyun Jeong, Kwang Bum Kim, Solid State Ionics 159 (2003) 223–232.
[26] Yoon Seok Jung, Peng Lu, Andrew S. Cavanagh, Chunmei Ban, Gi-Heon Kim, Se-Hee Lee, Steven M. George, Stephen J. Harris, Anne C. Dillon, Adv. Energy Mater. 3 (2013) 213–219.
[27] Yong Jeong Kim, Jaephil Cho, Tae-Joon Kim, Byungwoo Park, J. Electrochem. Soc. 150 (2003) A1723–A1725.
[28] Yang-Kook Sun, Chong Seung Yoon, Seoung-Taek Myungc, Ilias Belharouakd, Khalil Amine, J. Electrochem. Soc. 156 (2009) A1005–A1010.
[29] Ying Bai, Kai Jiang, Shuwei Sun, Qing Wu, Xia Lu, Ning Wan, Electrochim. Acta 134 (2014) 347–354.
[30] Sujith Kalluri, Moonsu Yoon, Minki Jo, Suhyeon Park, Seungjun Myeong, Junhyeok Kim, Shi Xue Dou, Zaiping Guo, Jaephil Cho, Adv. Energy Mater. (2016) 1601507.
[31] Artur Tron, Yeong Don Park, Junyoung Mun, J. Power Sources 324 (2016) 360–364.
[32] Hye Jin Lee, Yong Joon Park, Solid State Ionics 230 (2013) 86–91.
[33] H. Umehara, M. Takaya, S. Terauchi, Surf. Coating. Technol. 169–170 (2003) 666–669.
[34] Graham Beamson, David Briggs, High Resolution XPS of Organic Polymers, Wiley, 1992.
[35] K. Hamrin, G. Johansson, U. Gelius, C. Nordling, K. Siegbahn, Phys. Scripta 1 (1970) 277.
[36] Nam-Soon Choi, Jung-Gu Han, Se-Young Ha, Inbok Park, Chang-keun Back, RSC Adv. 5 (2015) 2732–2748.
[37] V.I. Nefedov, A Buslaev Yu, V Kokunov Yu, Zh. Neorganicheskoj Khim. 19 (1974) 1166–1169.
[38] G.E. Murch, R.J. Thorn, J. Phys. Chem. Solid. 41 (1980) 785–791.
[39] Ralf Wagner, Benjamin Streipert, Vadim Kraft, Jiménez Antonia Reyes, Stephan Röser, Johannes Kasnatscheew, Dennis Roman Gallus, Markus Börner, Christoph Mayer, Heinrich Franz Arlinghaus, Martin Korth, Marius Amereller, Isidora Cekic-Laskovic, Martin Winter, Adv. Energy Mater. 3 (2016) 1600096.
[40] Robert Black, Si Hyoung Oh, Jin-Hyon Lee, Taeeun Yim, Brian Adams, F. Linda, Nazar, J. Am. Chem. Soc. 134 (2012) 2902–2905.
[41] Maccone Patrizia, Brinati Giulio, Arcella Vincenzo, Polym. Eng. Sci. 40 (2000) 761–767.
[42] D. Aurbach, I. Weissman, A. Zaban, P. Dan, Electrochim. Acta 45 (1999) 1135–1140.
[43] S.F. Lux, I.T. Lucas, E. Pollak, S. Passerini, M. Winter, R. Kostecki, Electrochem. Commun. 14 (2012) 47–50.
[44] K. Edström, T. Gustafsson, J.O. Thomas, Electrochim. Acta 50 (2004) 397–403.
[45] Joseph K. Papp, Jason D. Forster, Colin M. Burke, Hyo Won Kim, Alan C. Luntz, Robert M. Shelby, Jeffrey J. Urban, Bryan D. McCloskey, J. Phys. Chem. Lett. 8 (2017) 1169–1174.
[46] Xiuyun Zhao, Svetlana Niketic, Chae-Ho Yim, Jigang Zhou, Jian Wang, Yaser Abu-Lebdeh, ACS Omega 3 (2018) 11684–11690.
[47] Robert R. Gagne, Carl A. Koval, George C. Lisensky, Inorg. Chem. 19 (1980) 2854–2855.
[48] V. Andriy, Plakhotnyk a, Ludger Ernst b, Schmutzler Reinhard, J. Fluorine Chem. 126 (2005) 27–31.